OBLIQUE-INCIDENCE SECONDARY EMISSION FROM CHARGED DIELECTRICS*

James W. Robinson and Paul A. Budd
The Pennsylvania State University

SUMMARY

Secondary electron emission coefficients have been measured on FEP-Teflon for normal and oblique incidence in the presence of a normal electric field. Such measurements require knowledge of the electrostatic environment surrounding the specimen, and they require calculation of particle trajectories such that particle impact parameters can be known. A simulation using a conformal mapping, a Green's integral, and a trajectory generator provides the necessary mathematical support for the measurements, which have been made with normal fields of 1.5 and 2.7 kV/mm. When incidence is normal and energy exceeds the critical energy, the coefficient is given by $(V_0/V)^{.58}$, and for oblique incidence this expression may be divided by the cosine of the angle. The parameter V_0 is a function of normal field.

INTRODUCTION

Experimental measurements of secondary electron emission coefficients (SEEC) for FEP-Teflon are reported here. Two features of the work make it unique. Measurements made on a charged specimen are affected by the surface field, and they are made at oblique incidence such that trajectories are influenced by the electric fields. Two activities, experimental measurements and computer simulation, have been combined into a complementary procedure which yields the desired results. The simulations, which have been described in reference 1, are reviewed here briefly, and typical measurements are described.

Previous Work

Katz et al (ref. 2) have developed a spacecraft charge modelling code NASCAP which uses a functional form for SEEC similar to the straggling theory presented by Lye and Dekker (ref. 3). They also use a functional dependence for angle of incidence similar to that proposed by Jonker (ref. 4). Yet experimental measurements have generally not been available. Quoc-Nguyen (ref. 5) measured SEEC in normal fields for normal incidence, finding that the

---

*The authors gratefully acknowledge the support of this work by The National Aeronautics and Space Administration under Grant NSG-3166.

critical point for unity emission is a function of surface field. This report is a direct extension of the work initiated by him.

Procedures

The specimen of 0.12-mm FEP-Teflon is placed on a flat grounded platform which may be rotated in a cylindrical shell as illustrated in figure 1. The specimen is oriented normal to the flux from a mono-energetic flood gun and the cylinder is rotated so that a window is placed above the specimen. After a steady state is reached, the flood gun is turned off and the cylinder is again rotated so that the specimen is enclosed in a well defined electrostatic environment. The specimen holds its charge for long periods of time; decay during an experiment is negligible. Discharging is done by exposing the specimen to the flood gun while the flood gun potential is gradually reduced.

The distribution of charge on the specimen is determined from an assessment of electron trajectories which come near to but do not strike the specimen. The probing beam, which is injected through a slot in the cylinder, has a width less than 0.2 mm and provides highly resolved measurements. When the beam does not strike the specimen, it usually reflects back to the cylinder where it is detected with fine probe wires. Measurements of beam exit positions for various injection points and injection velocities provide a basis for determining the potential distribution on the specimen. The simulations are important in this phase of the work.

Once the distribution of potential is known, impacting trajectories can be simulated for the purpose of calculating impact point, impact angle, and impact velocity. This information is crucial for interpreting the measurements of SEEC. Though SEEC is relatively easy to measure, a measured value is of worth only when the impact parameters are known.

The actual measurements of SEEC are accomplished by directing an electron pulse of known charge (about 1pC) at the specimen and detecting a change of charge induced in the metal substrate behind the specimen. If these charges are designated as Q_i and Q_s, then the SEEC is

$$\sigma = 1 - Q_s/Q_i \tag{1}$$

This definition collects backscattering, inelastic scattering, and the low-energy SEEC into a single parameter.

SIMULATION

The geometry of the experimental system, a half-cylinder, was chosen for several reasons, one being experimental convenience. However the choice was primarily related to the need for simulating the experimental system with a numerically efficient process. The use of a sufficiently long specimen (at least equal to the diameter) allowed calculations to be done in two instead of

three dimensions, and consequently, a technique using conformal mapping could be applied. By this method, the half-cylinder was easily converted to a half-plane where a Green's integral yielded electric potential. Repeated applications of this technique provided the data needed by particle trajectory tracing routines. The methods described here have been developed by Quoc-Nguyen (ref. 5) and Robinson and Tilley (ref. 6), and they have been adapted to this geometry by Robinson (ref. 1).

Conformal Mapping

If the radius of a semicircle in the upper half plane W is A then the mapping

$$Z = 2W/\{1+(W/A)^2\} \tag{2}$$

converts that semicircle into the upper half plane Z by opening it at the point W=iA. The potential of a point is the same in either plane but fields computed in the Z plane must be transformed according to the equations

$$\begin{aligned} E_u &= SE_x + TE_y \\ E_v &= -TE_x + SE_y \end{aligned} \tag{3}$$

where S and T are defined by

$$dZ/dW = S + iT. \tag{4}$$

Green's Integral, Surface Potential, and Fields

In the Z-plane the potential at some point (X,Y) is given by an integral over the specimen's surface where potential on the surface is designated P′(X). The integral is

$$P(X,Y) = \frac{Y}{\pi}\int_{-B}^{B} \frac{P'(X')\,dX'}{(X-X')^2+Y^2} \tag{5}$$

The surface potential P′(X) has been expressed for this work as a polynomial in X, the transformed variable, rather than being expressed in terms of U. The expression is

$$P'(X) = \sum_{i=0}^{m} A_i (X/B)^i \tag{6}$$

where m is finite. It has been assumed that P′(-B)=P′(B)=0 and that, consequently, the sum of even A_i's is zero and the sum of odd A_i's is zero. It is experimentally convenient that A_0 is the potential at the center of the

specimen. Furthermore all of the odd A_i values are zero when the potential is symmetric about the origin, a common though not necessary experimental condition.

When the expression for surface potential is substituted into the Green's integral, the resulting expression may be written as

$$P(X,Y) = (Y/\pi) \Sigma \ (A_i I_{1i}/B^i) \qquad (7)$$

where

$$I_{1i} = \int_L^H \frac{(R+X)^i dR}{(R^2+Y^2)} \qquad (8)$$

and where L=-B-X and H=B-X. Electric field components are found from the negative gradient of the potential and are

$$E_x = -(2Y/\pi) \Sigma \ (A_i I_{2i}/B^i)$$
$$E_y = -P/Y + (2Y^2/\pi) \Sigma \ (A_i I_{3i}/B^i) \qquad (9)$$

where the integrals are

$$I_{2i} = \int_L^H \frac{R(R+X)^i \, dR}{(R^2+Y^2)^2} \qquad (10)$$

$$I_{3i} = \int_L^H \frac{(R+X)^i \, dR}{(R^2+Y^2)^2} \qquad (11)$$

Typically one specifies the radius A, the specimen width B (as measured in the conformed plane), the coefficients A_i, and some point (U,V). Then a direct procedure may be followed to obtain the required results. A conformal mapping yields the point Z (or X,Y) and the three integrals are evaluated. Field components so obtained are then mapped back to the original W plane.

In the limit as $Y \to 0$, the integrals diverge, but an analytical limiting procedure can be applied to obtain equations for the fields on the surface of the specimen.

DeVogelaire's Method

This method, which is used to generate particle trajectories, applies to second order differential equations without explicit first derivatives (ref. 7). It is correct to fourth order and uses a relatively simple stepping procedure. The coordinates and velocity components must be known at some time t_i and also the coordinates must be known at the time corresponding to a half-step before t_i. Field components are calculated at these points. Then, for the U-motion, a new half-step (designated by h) is taken with

$$U_h = U_i + V_u T/2 + QT^2((3+F)E_u - FE_{-hu})/24 \quad (12)$$

where T is the time step, U is coordinate, V is velocity, E is field, and Q is the charge/mass ratio. Usually F may be considered to be unity, though it is assigned a different value when a change of time step is implemented. After the half-step, the fields at the new point are evaluated and the whole step is completed with

$$U_{i+1} = U_i + V_u T + QT^2(E_u + 2E_{hu})/6 \quad (13)$$

Equations similar to these are used simultaneously for stepping in the V-direction. After a step has been completed the new velocities are evaluated from the U-equation

$$V_{u,i+1} = V_u + QT(E_u + 4E_{hu} + E_{u,i+1})/6 \quad (14)$$

and from a similar V-equation. The stepping procedure is repeated as many times as needed to trace the complete trajectory.

As the particle approaches the specimen the time increment is reduced by a factor of 4. This is done by defining the factor F to have a value 1/4 for the next step only and by redefining the time step with T=FT. Likewise for particles leaving the region close to the specimen F is set equal to 4 for one time step only to cause an increase in the size of the time step.

Special procedures are required when the trajectory runs into a boundary. When the particle approaches the plane of the specimen a branch occurs so that the trajectory can be ended precisely on the plane. This is done by calculating the value of time step required for the last step and then by using that time step in the usual formulas. The trajectory may also intersect the circular boundary. In this case the trajectory at the last point inside the boundary is linearly extended until the boundary is crossed.

Two different subroutines have been developed to start two different types of trajectory. In each case the given point which represents injection of a particle is treated as a preceding half step and the reference point is generated by appropriate equations which take an initial half step. One calculation starts from the circular boundary and corresponds to particles injected at that boundary. The other starts on the surface of the specimen and allows the user to specify conditions at that end of the trajectory, which is traced backwards from the specimen to the cylinder.

The trajectory tracing routines have been executed many times for a variety of conditions. Figure 2 shows typical impacting trajectories for which the specimen potential varies as

$$P' = 1-(X/B)^6 \quad (15)$$

and for which the particle energy is 1.56 times the potential at the center of the specimen. Figure 3 shows particles which have energy of 0.85 times the

potential at the center of the specimen.

EXPERIMENTAL PROCEDURES

The system, shown in figure 1, was placed in a stainless bell jar and evacuated by a turbomolecular pump to a pressure below the gauge limit of 10^{-6} torr. Continuous pumping and operation of filaments for days at a time assured stable and reproducible measurements. Both specimen platform and cylinder were rotated with stepper motors which took 200 steps/revolution. One step corresponded to a motion of 0.8 mm at the periphery of the cylinder. This system could be used in a variety of modes for measuring non-impacting trajectories, specimen surface potentials, and SEEC for impacting trajectories. In an auxiliary series of measurements a small Faraday cup was placed on the platform next to the specimen so that reference measurements of SEEC could be made for the conditions that surface potential was zero and that incidence was normal.

Probing Beam

The beam was a versatile tool for making the various measurements of interest. It was admitted to the cylinder through a slot cut in the cylinder such that no matter how it rotated, the beam was not blocked. The beam itself was shaped by slits and aperture plates so that it had a cross section of about 2x0.2 mm. The longer dimension was oriented parallel to the axis of the cylinder, and the beam was deflected in the direction of the shorter dimension. Sensor wires, mounted at the slot of the cylinder, rotated with the cylinder and detected the beam either where it entered or where it exited, if indeed it did return to the cylinder.

The beam was deflected by applying voltage between deflection plates which were located behind the beam orifice. Either steady state or pulsed voltages could be applied, the steady state being more useful for beams returning to the cylinder and the pulse being useful when the specimen was to be struck briefly with a measurable packet of charge. A typical pulse duration was 1 ms though for some cases much longer pulses were used. Typical beam current was 1nA and a typical charge packet was 1pC. By measuring deflection voltage required to move the beam from one sensor wire to another, one could determine the deflection factor and thus correlate simulated and experimental deflections.

The mechanical alignment of the gun was not perfect but that problem was easily resolved by assigning the condition of normal incidence to be that deflection voltage for which a beam returned to its point of origin. This condition was for a charged specimen which was rotated so that it faced the beam.

Surface Potential

The peak surface potential, which is represented by A_0, is determined experimentally before computer simulations can be attempted. When the surface has been charged with a flood gun potential of V_f then the difference, $V_f - A_0$, is equal to the critical voltage for which the SEEC is unity. This value is influenced by surface field strength which in turn is related to sample width; it was 6 mm for this work. The surface potential was defined experimentally to be the lowest possible probing beam accelerating potential for which any perturbation in surface charge (or substrate charge) could be noted. Normal incidence at the center of the specimen is required for this measurement. Table 1 shows results of several such measurements and it also shows normal electric field E_v at the center of the specimen.

When A_0 was determined, then trajectories of the form shown in figure 3 could be compared with experimentally measured trajectories. The end points of the trajectories were the quantities compared. Figure 4 illustrates this comparison for a specimen originally charged with a 10kV flood beam. The various curves correspond to different choices of the exponent M in the expression

$$P' = A_0\{1-(X/B)^M\}, \tag{16}$$

and consequently, for this case M should be 4 for a best fit. More elaborate functions could be used for P′ but for the study of incidence on the center of the specimen, further refinements were not incorporated.

SEEC for Uncharged Specimen

The experimental system does not contain provisions for measuring the charge packet delivered by the pulsed probing beam. Consequently several measurements were made with a small Faraday cup inserted above the specimen platform and offset slightly so that the beam could be directed alternately at the specimen and the cup. These measurements were made at normal incidence with the surface of the specimen discharged so that beam trajectories could be assumed to be straight lines. When such measurements had been completed, the SEEC could be computed, and the values so determined could be used for calibrating the beam in the absence of the cup.

For this series only, Q_i was measured with the cup and Q_s was the charge induced in the substrate when the beam struck the specimen. Then equation 1 was applied and the SEEC so calculated were represented by

$$\sigma = (V_0/V)^N = (Q_i - Q_s)/Q_i \tag{17}$$

where $V > V_0$, V_0=1.5kV, and N is approximately constant. Table 2 shows recorded data and the corresponding values of N. It has been assumed that N=0.58 for normal incidence on the uncharged specimen, and this value is used in calibrating all other measurements.

SEEC for Charged Specimen

With no Faraday cup present, the specimen is charged and struck with a charge packet from the probing beam. Thus Q_s is measured for whatever surface potential and angle of incidence are of interest. Then the surface is discharged and struck again at normal incidence. From this second measurement, Q_i is determined by using equation 17 and the assumed value of N. Finally the SEEC is calculated from equation 1.

One requirement is that the injection point and injection velocity be carefully calculated so that the impact parameters will be as desired. The simulation of trajectories provides the necessary data yet an uncertainty does exist as to the value of deflection plate voltage which corresponds to a radial injection of the beam. Ideally this voltage would be zero yet slight misalignment can cause it to be different. Data shown later illustrate this problem which, though not serious, might be alleviated by breaking the metal backing of the specimen into two zones. Then the transition point between zones could be precisely located in terms of deflection plate voltage.

Another requirement is that the charge packet be sufficiently small that the surface potential changes little. If a second response at the same spot is smaller than the first, then the pulse size is too large. Larger pulses could be used when the SEEC was close to unity than otherwise because Q_s was zero at the unity condition. The challenge of measuring with small charge packets was to establish conditions where drift and noise associated with the electrometer measurement did not obscure the data. One source of noise may be micro-discharges on the surface of the specimen; noise was greater on a charged specimen than on an uncharged specimen. Cleanliness is also important. Drifting generally could be controlled by carefully shielding the critical hardware from the charged particle environment created by the electron beam sources.

EXPERIMENTAL DATA

Measurements have been made for values of V_f shown in table 1 of 8 and 12 kV where angles of incidence have ranged as high as 70 degrees. First it is noted that the form of equation 17 is appropriate for normal-incidence data if N=0.58 and V_0 is 1.85 kV for a surface potential of 6.15 kV (or 1.96 kV for 10.04 kV). Figure 5 illustrates the function and shows superimposed data points for the case where surface potential is 6.15 kV. These normal incidence measurements are made in the center of the specimen, yet location of the precise center is not critical as the measured SEEC is insensitive to the point at which the measurement is made. This is because the potential function has a broad maximum in the center and also because slight deviations from normal incidence are inconsequential.

Also shown in figure 5 are curves for angles of incidence θ which were obtained by dividing equation 17 by $\cos(\theta)$ according to the usually assumed

theory (ref. 4). These theoretical curves were used in constructing figure 6 which illustrates measurements at oblique incidence.

All of figure 6 was generated from simulation and the assumed theoretical dependence upon θ except for the data points which have been superimposed. Except for an obvious lateral shift of data points, which is related to establishing a reference deflection voltage, the match between theory and data is excellent. The data points themselves are easily located on the figure in terms of the experimental parameters of Q_s, Q_i, and deflection voltage. However some additional explanations are needed for the calculated curves. The experiment was simulated by assuming a form for P' with an exponent of 6 as shown in equation 15. It was also assumed that the parameters from table 1 for V_f=8 were appropriate. Finally it was assumed that the impacting beam had an energy of 9.5 keV as was the case for the experiment. The injection point for the beam was chosen to cause a 45-degree impact angle at the center of the specimen and then numerous beams were simulated where the deflection angle of the beam was varied, as shown in figure 2. Figure 6 shows the surface potential of the specimen, the impact position for each of several simulated beams, the impact angles of each of those beams, and deflection plate voltages corresponding to each of the simulated beams. Then from figure 5 the secondary emission coefficient was calculated for combinations of surface potential and angle of incidence. The data shown in figure 6 is typical of many measurements which have been made. Its characteristic is that the measured SEEC is much larger off center, where angle of incidence is greater, than in the center where the impact energy is lowest. It should be noted here that the side of the specimen shown is the side opposite from the beam source. The impacts on the near side of the specimen are at lesser angles of incidence and the values of SEEC are corresponding lower. Field strength is of course not constant over the range of data shown but for this case one may assume it to be reasonably constant out to 2 mm where the tangential component becomes significant.

Figure 5 indicates that for angles of 70 degrees or more, the critical point may be as high as 10 kV. This has indeed been demonstrated by measurements with both of the previously specified charging conditions.

REFERENCES

1. Robinson, J. W.: Mapping of Electrical Potential Distribution with Charged Particle Beams. NASA Grant NSG-3166, The Pennsylvania State University, September 1980.

2. Katz, I. et al: A Three Dimensional Dynamic Study of Electrostatic Charging in Materials, NASA CR-135256, August 1977.

3. Lye, R. G.; Dekker, A. J.: Theory of Secondary Emission. Phys. Rev. 107,4, pp977-981, August 1957.

4. Jonker, J. L. H.: On the Theory of Secondary Electron Emission. Phillips Research Reports 7, pp1-20, 1952.

5. Quoc-Nguyen, N.: Secondary Electron Emission from a Dielectric Film Subjected to an Electric Field. NASA CR-155213, November 1977.

6. Robinson, J. W.; Tilley, D. G.: Potential Mapping with Charged Particle Beams. Spacecraft Charging Technology-1978, pp 606-620, NASA Conference Publication 2071, 1979.

7. DeVogelaire, R.: A Method for the Integration of Differential Equations of Second Order Without Explicit First Derivatives. J. Res. National Bureau of Standards 54, 119 March 1955.

Table 1: Surface Potential, Critical Voltage, and Normal Field for Various Flood Beam Potentials

V_f (kV)	A_0 (kV)	V_c (kV)	E_v (kV/mm)
6.	4.2	1.8	0.98
8.	6.15	1.85	1.50
10.	8.08	1.92	2.09
12.	10.04	1.96	2.73
14.	12.0	2.0	4.08

Table 2: Measurements for the Uncharged Specimen

V (kV)	Q_s (pC)	Q_i (pC)	σ	N
4.0	6.00	12.8	0.53	0.61
5.0	6.25	12.8	0.51	0.55
6.5	3.30	5.75	0.43	0.58
8.0	2.25	3.75	0.40	0.55
10.0	6.50	4.20	0.34	0.57

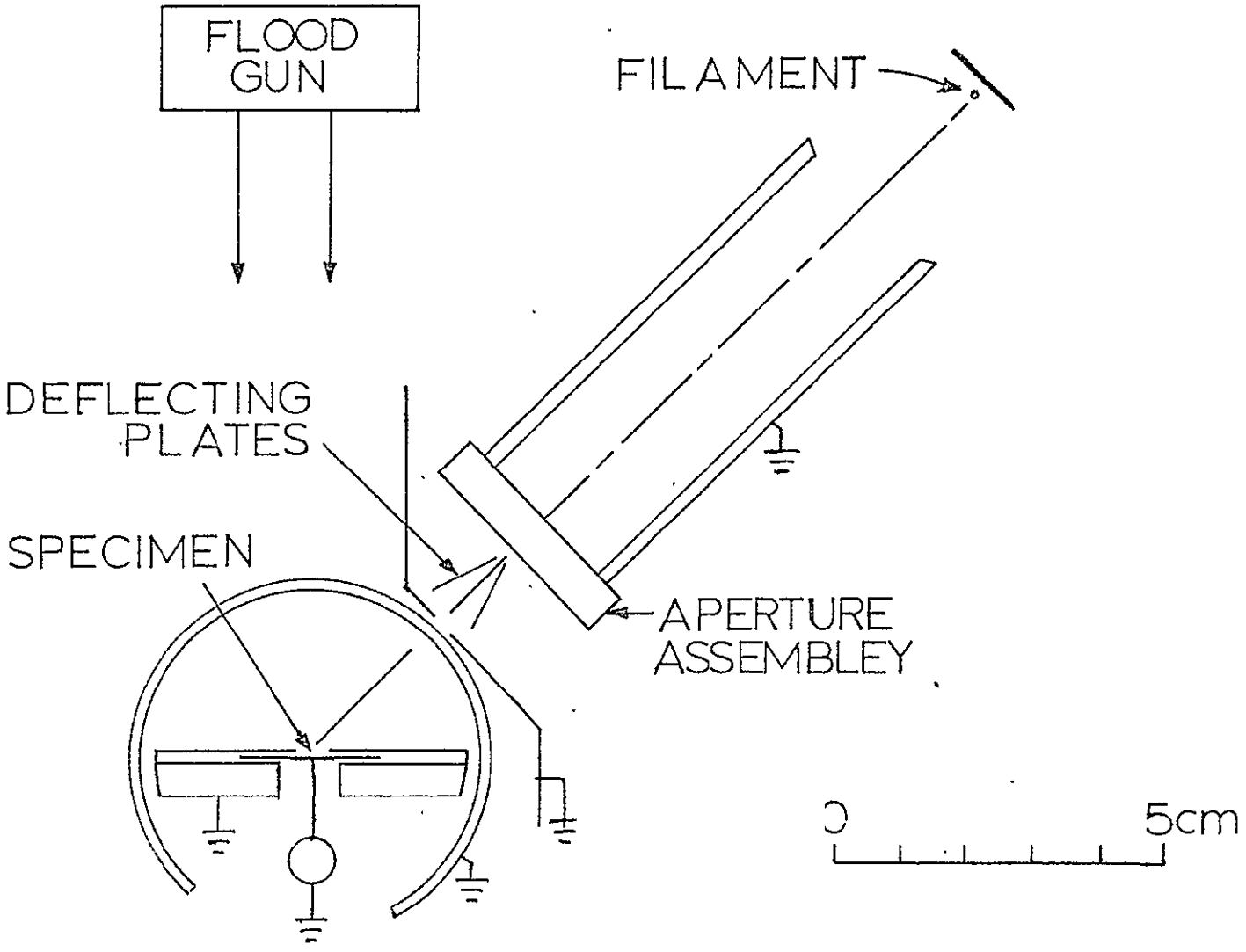

FIGURE 1. EXPERIMENTAL FACILITY

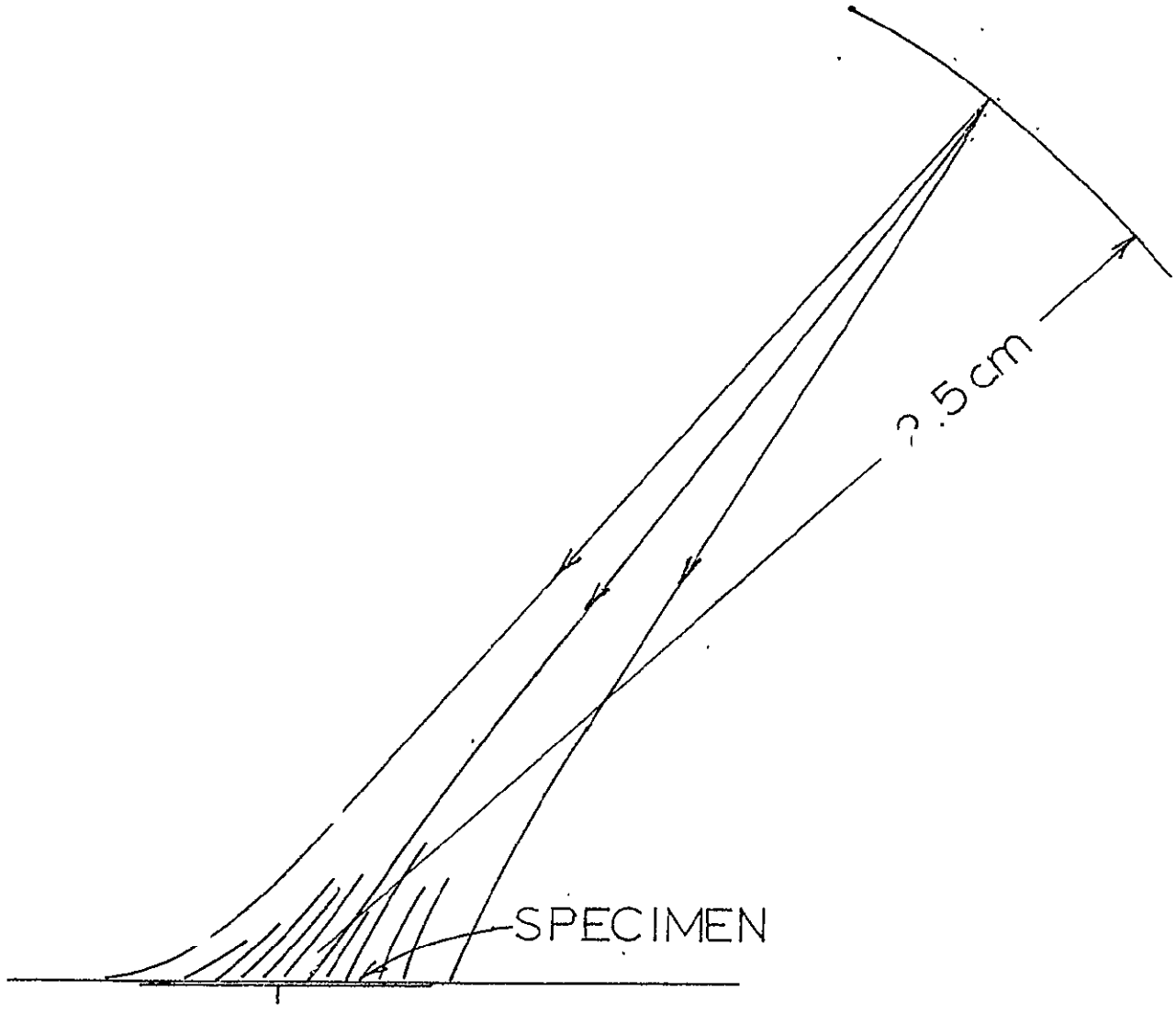

FIGURE 2. SIMULATED IMPACTING TRAJECTORIES

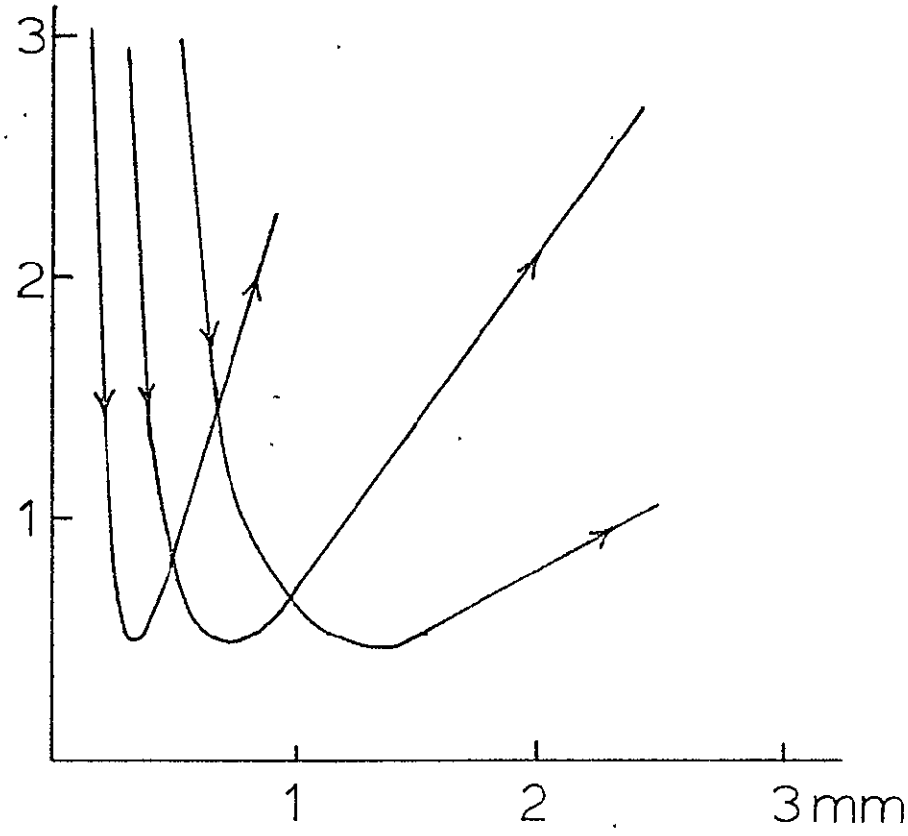

FIGURE 3. SIMULATED REFLECTING TRAJECTORIES

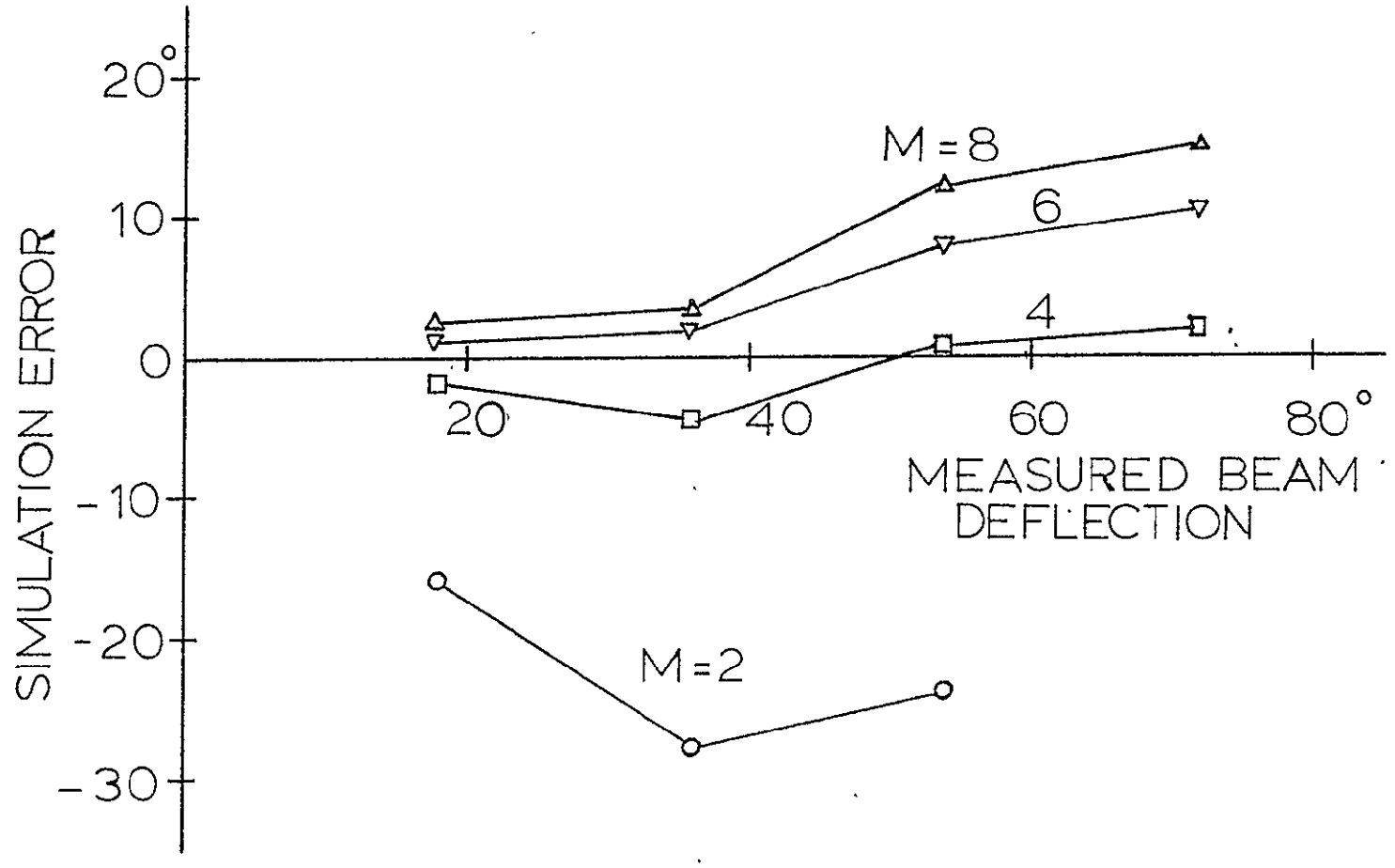

FIGURE 4. COMPARISON OF SIMULATION AND EXPERIMENT EOR DEFLECTED BEAMS

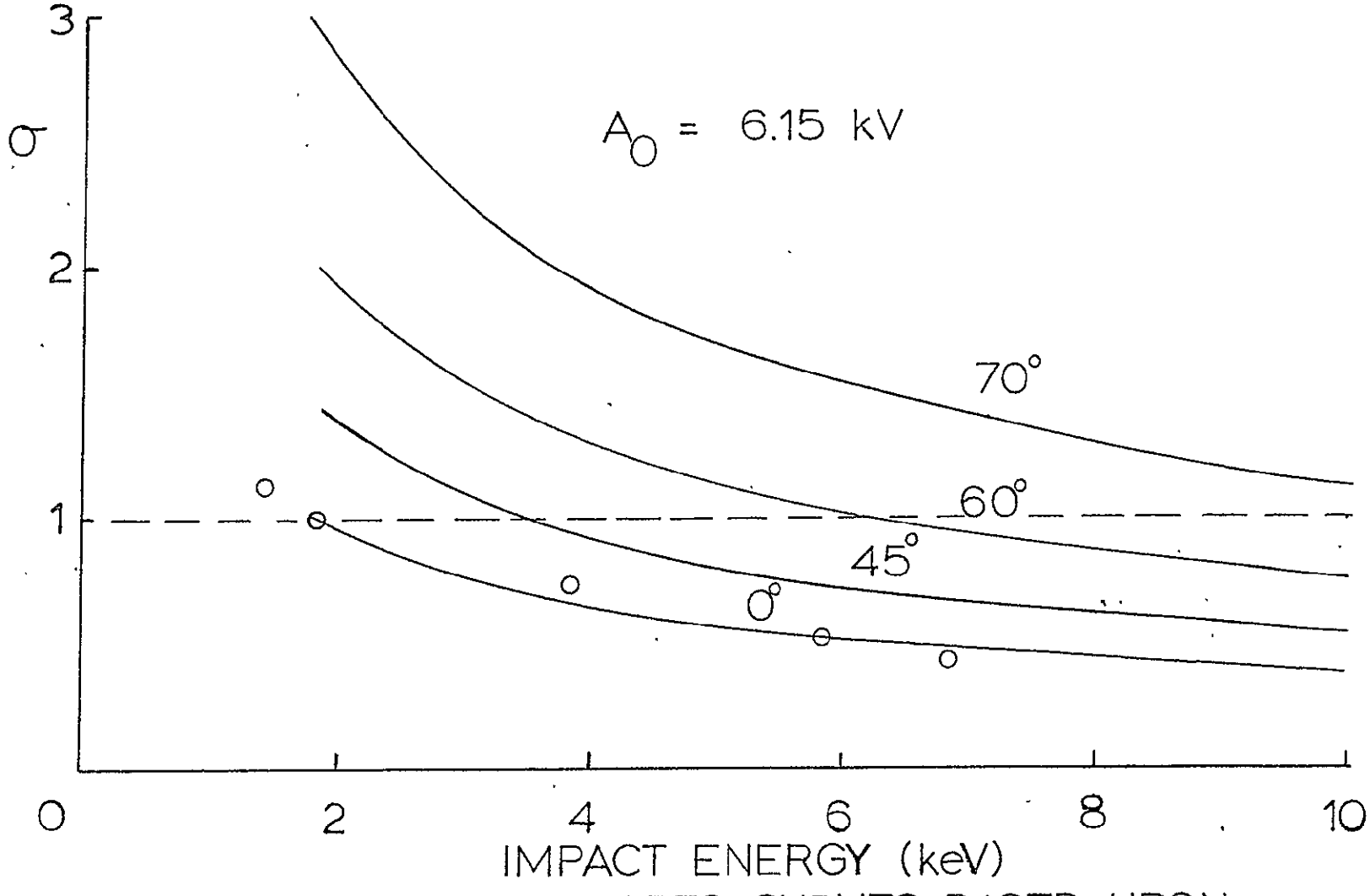

FIGURE 5. THEORETICAL SEEC CURVES BASED UPON NORMAL-INCIDENCE DATA

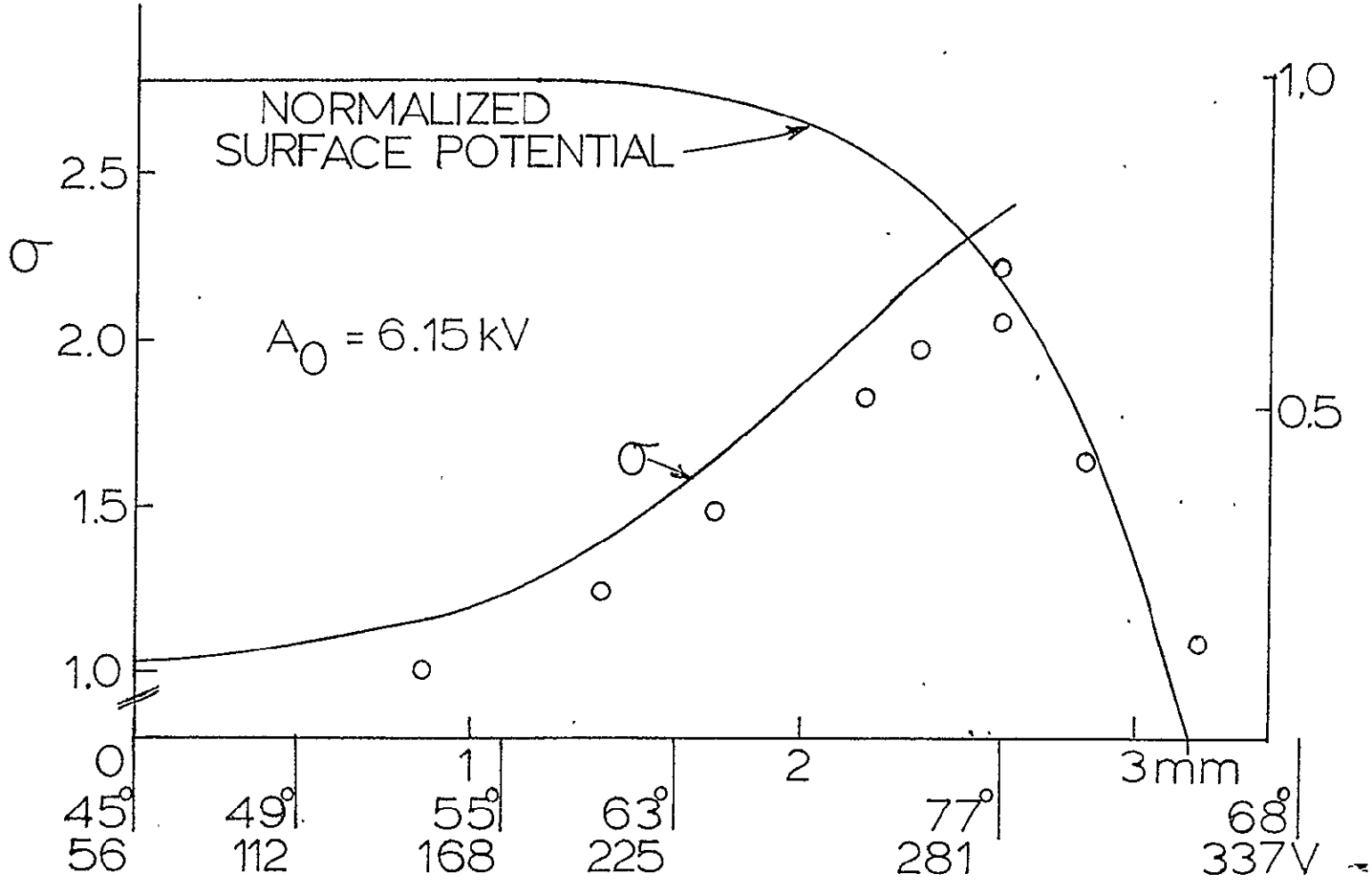

FIGURE 6. COMPARISON OF EXPERIMENTAL DATA WITH THEORY. SIMULATED TRAJECTORY PARAMETERS ARE INDICATED ON THE ABCISSA.